NANO LETTERS

pubs.acs.org/NanoLett

Letter

A Statistical Route to Robust SERS Quantitation Beyond the Single-Molecule Level

Hao Zhang,[#] Longkun Yang,[#] Meng Zhang, Hong Wei, Lianming Tong, Hongxing Xu,[*] and Zhipeng Li[*]

Cite This: *Nano Lett.* 2024, 24, 11116−11123

Read Online

ACCESS | Metrics & More | Article Recommendations | Supporting Information

ABSTRACT: Single-molecule surface-enhanced Raman spectroscopy (SM-SERS) holds great potential to revolutionize ultratrace quantitative analysis. However, achieving quantitative SM-SERS is challenging because of strong intensity fluctuation and blinking characteristics. In this study, we reveal the relation $P = 1 - e^{-\alpha}$ between the statistical SERS probability P and the microscopic average molecule number α in SERS spectra, which lays the physical foundation for a statistical route to implement SM-SERS quantitation. Utilizing SERS probability calibration, we achieve quantitative SERS analysis with batch-to-batch robustness, extremely wide detection range of concentration covering 9 orders of magnitude, and ultralow detection limit far below the single-molecule level. These results indicate the physical feasibility of robust SERS quantitation through statistical route and certainly open a new avenue for implementing SERS as a practical analysis tool in various application scenarios.

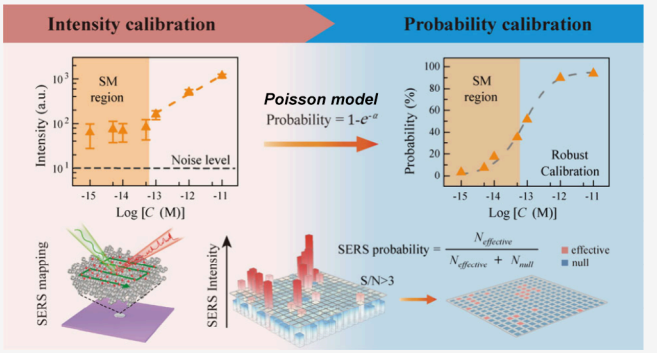

KEYWORDS: *surface-enhanced Raman spectroscopy, SERS, single-molecule detection, statistical SERS probability, Poisson distribution*

Quantitation at the few molecules level is a topic of significant scientific and practical interest in fields including chemical science, early diagnostics, food/environmental safety, etc.[1−4] Among various analytical techniques, such as enzyme-linked immunosorbent assays and polymerase chain reaction,[5,6] surface-enhanced Raman spectroscopy (SERS) is the most promising method for single-molecule detection (SMD) due to its combination of specificity of molecular "fingerprints" and sensitivity enormously enhanced by plasmonic "hot spots".[7−11] However, SERS signals highly rely on the contribution from a few molecules located within the hot spots,[12−15] whose enhancement ability is rather vulnerable to nanoscale variations in geometries.[16−21] These uncertainties make SERS signals irreproducible with the intensity even varying by several orders of magnitude,[22−24] posing a great challenge for implementing SERS quantitation under the framework of intensity gauging.[25−30] More seriously, in the ultralow concentration region ($\sim 10^{-13}$ M), when only several molecules or a single molecule contributes to the SERS spectrum, intrinsic intensity fluctuations (either temporal or spatial) occur due to the thermal-activated and light-activated blinking.[31−33] The measured SERS intensity would even lose its relevance to concentration changes. Quantitation of single-molecule surface-enhanced Raman spectroscopy (SM-SERS) through traditional intensity gauging becomes physically impossible.

As a critical step toward SM-SERS, statistical toolboxes have been developed to identify single-molecule signals and quantitation calibrations.[34−37] According to the Poisson distribution, the probability of measuring a certain number of molecules (n) in one spectrum follows the relation $p(n, \alpha) = \frac{\alpha^n}{n!} e^{-\alpha}$, where α is the average number of molecules measured per spectrum under a certain concentration C. However, the attempt to identify α through the observation of Poisson distribution in SERS intensity is practically infeasible, because statistics of SERS intensity in the single-molecule concentration region change to Pareto-type distribution due to the strong intensity fluctuation.[34,38] Therefore, a bianalyte approach based on Poisson-binomial distribution was proposed as a reliable method to identify single-molecule events,[39−41] which illuminated a statistical route to quantitative SERS.[35] However, quantifying analytes of an unknown concentration is impossible by the bianalyte method.

Received: July 22, 2024
Revised: August 3, 2024
Accepted: August 5, 2024
Published: August 8, 2024

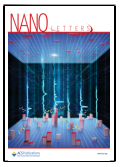

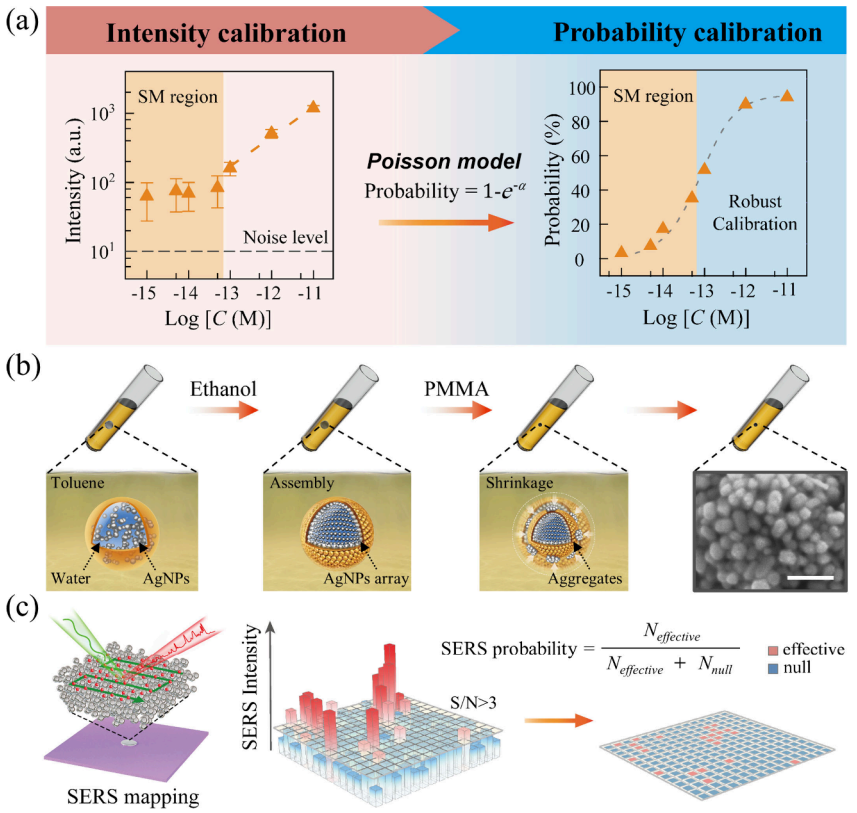

Figure 1. SERS quantitation through statistical probability. (a) Intensity calibration vs statistical probability calibration. Left panel: SERS intensity of CV as a function of concentration. Right panel: SERS probability as a function of concentration. (b) Sketch of the 3D AgNP aggregate preparation. From left to right: AgNP colloid in toluene; assembly of AgNPs on toluene/water interface; shrinkage of AgNP array; typical SEM image of AgNP aggregates. The scale bar is 200 nm. (c) Scheme of SERS mapping and extracting SERS probability from SERS intensity mapping. Effective events were counted as pixels with signal-to-noise $S/N > 3$ in the SERS mapping. Mapping measurements with step size 1 μm were performed under the excitation of a 532 nm laser with power density 19 $\mu W/\mu m^2$ and acquisition time 1 s, if not stated otherwise.

In this work, we propose a statistical route to SM-SERS quantitation by gauging SERS probability (Figure 1a). We found that SERS probability can sensitively respond to concentration changes even below the single-molecule level. We realized batch-to-batch SERS quantitation down to femtomolar which was 2 orders of magnitude lower than the single-molecule threshold, demonstrating the robustness of SERS probability calibration. More importantly, the physical foundation for the statistical SERS quantitation was well established by correlating the measured SERS probability and the average molecule number α determined from bianalyte analysis. We also extended this statistical quantitative approach to various SERS substrates, which enabled reliable and flexible biochemical quantitative analysis with a concentration range covering 9 orders of magnitude. These results not only deepen our understanding about the stochastic nature of SM-SERS but also reveal the physical feasibility of implementing statistical SERS quantitation.

SM-SERS was realized based on three-dimensional (3D) aggregates of silver nanoparticles with high enhancement and uniformity, which were fabricated by assembling silver nanoparticles at the water−toluene interface and then shrinking the droplet (see Materials and Methods in the Supporting Information and Figure 1b). The scanning electron microscopy (SEM) images show that the 3D aggregates are composed of highly packed silver nanoparticles with an average size of ∼75 nm (Figure 1b and Figure S1). The 3D aggregates were then transferred onto a silicon wafer, which was immersed into a crystal violet (CV) solution for 2 h and dried under ambient conditions for SERS measurements. The performance of the assembled 3D aggregates was verified by mapping the SERS of CV under the excitation of a 532 nm laser (details of spectral measurements are given in the Materials and Methods in the Supporting Information). As shown in Figure 1a, the SERS intensity of CV (914 cm^{-1}) can respond to the concentration change from 10^{-11} M to 10^{-13} M. This linear relationship is usually used as the calibration curve for traditional intensity-based quantitation.[42] For higher concentrations, it saturates after 10^{-7} M indicating the full coverage of molecules, which can be described by the phenomenological Hill equation (Figure S2). However, at extremely low concentrations $<10^{-13}$ M, the SERS intensity thoroughly lost the relevance to concentrations (shadow area in Figure 1a). This phenomenon was also confirmed in previous SERS measurements when single or a few molecules contributed to SERS signals.[43] This intrinsic nature of single-molecule spectra inevitably ruins the physical foundation of quantitation by traditional $I-C$ (intensity−concentration) curves. Hence, we resorted to the SERS probability (P) as a new gauging quantity. In statistics, the probability of acquiring SERS signals is defined as the ratio between all effective counts and the total number of measurements that contain null events.[43,44] Experimentally, SERS probability can be computed by counting the effective pixels (signal-to-noise (S/N) > 3) in the mapping image (Figure 1c),

https://doi.org/10.1021/acs.nanolett.4c03507
Nano Lett. 2024, 24, 11116−11123

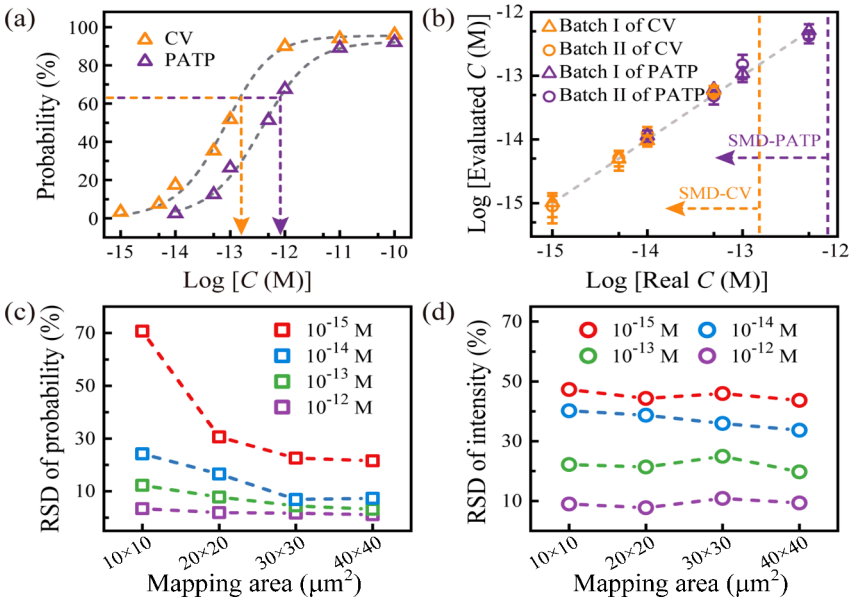

Figure 2. SERS probability and quantitative detection. (a) SERS probability as a function of concentration for CV (914 cm^{-1}, orange triangles) and PATP (1078 cm^{-1}, purple triangles). Gray dashed lines are plotted to guide eyes. Orange and purple dashed arrows indicate the SM-SERS thresholds for CV and PATP, respectively. SERS probabilities at different concentrations were obtained from 900 SERS spectra with mapping area 30 × 30 μm^2 and step size 1 μm. (b) Evaluated values for solutions of different concentrations by using the probability−concentration relation in panel a. Orange and purple data correspond to CV and PATP, respectively. Gray dashed line "$y = x$" is plotted to guide eyes. Orange and purple vertical dashed lines denote the SMD threshold for CV and PATP, respectively. The error bars are standard deviations obtained from four evaluations. (c) Relation between RSD of SERS probability and mapping areas under different concentrations of CV. (d) Relation between RSD of SERS intensity and mapping areas for the same samples in panel c.

$$P = \frac{N_{\text{effective}}}{N_{\text{effective}} + N_{\text{null}}}$$

where $N_{\text{effective}}$ and N_{null} are the numbers of effective and null pixels, respectively. As shown in Figure 1a, although SERS intensity loses relevance to concentration change below 10^{-13} M, probability P can still sensitively respond to concentration even down to 10^{-15} M. This phenomenal feature is the quantitative basis of statistical SERS probability, which offers a unique approach to implement SM-SERS quantitation.

We first quantify the CV solution by building the SERS probability calibration curve, as shown by the orange triangles in Figure 2a (mapping data in Figure S3). Then, two batches of extremely diluted CV solutions with concentrations ranging from 10^{-15} M to 0.5 × 10^{-13} M were evaluated. By measuring the SERS probability of the to-be-evaluated CV solutions (mapping data in Figure S4) and interpolating the calibration data in Figure 2a, we successfully obtained the concentrations of the samples (orange triangles/circles in Figure 2b). For example, for CV with a concentration of 1 × 10^{-14} M, the evaluated concentrations for two batches of solution were (0.9 ± 0.2) × 10^{-14} M and (1.2 ± 0.3) × 10^{-14} M, respectively. Both values correctly recovered the real concentration. For two batches of CV solution at 10^{-15} M, the concentrations were evaluated to be (1.0 ± 0.4) × 10^{-15} M and (0.9 ± 0.4) × 10^{-15} M, respectively, further demonstrating the successful quantitation of extremely dilute solutions. The reproducible quantitation from batch to batch also indicates the robustness of the statistical SM-SERS quantitation. It is known that SM-SERS of molecules with smaller Raman cross sections is more challenging. Here we also demonstrated the quantitative detection of *p*-aminothiophenol (PATP), a molecule with a relatively smaller Raman cross section.[45] First, as shown in Figure 2a, the calibration curve of probability−concentration is built by employing the same mapping procedure (30 × 30 μm^2, step size 1 μm, mapping data in Figure S5). Then, two batches of PATP solutions with concentrations ranging from 10^{-14} M to 5 × 10^{-13} M were evaluated (mapping data in Figure S6). As shown by the purple triangles and circles in Figure 2b, different concentrations of PATP were successfully evaluated. For example, two batches of solution with concentration of 10^{-14} M were well recovered at (1.0 ± 0.2) × 10^{-14} M and (1.3 ± 0.2) × 10^{-14} M, respectively.

Furthermore, a lower relative standard deviation (RSD) is critical to the accuracy of quantitative measurements. The RSD of probability can be effectively suppressed by increasing the number of spectra involved in statistics,[46] i.e., increasing the mapping area, as shown in Figure 2c. At a concentration of 10^{-15} M, the RSD of statistical SERS probability is substantially reduced from 70% at 10 × 10 μm^2 to 25% at 30 × 30 μm^2, and further to 21% at 40 × 40 μm^2. For higher concentrations, such as 10^{-13} M, the RSD can be well controlled below 5% (30 × 30 μm^2). In contrast, the RSD of the SERS intensity is almost independent of the mapping area (Figure 2d). Even worse, it increases rapidly to 45% for 10^{-15} M, where quantitation through SERS intensity would lose its accuracy and feasibility. Compared with intensity-based quantitation, the probability route shows superiority on the precision of SERS quantitation.

Establishing a sound physical foundation for statistical SM-SERS quantitation is a critical step toward reliable applications. Since SERS probability only counts the active and inactive SERS events, it is governed by Poisson distribution rather than the Pareto-type distribution.[34,47] According to the Poisson distribution, the SERS probability P can be modeled by $\sum_{n=1}^{\infty} p(n,\alpha)$, which represents the probability of detecting at least one molecule. Then SERS probability can be expressed as

https://doi.org/10.1021/acs.nanolett.4c03507
Nano Lett. 2024, 24, 11116−11123

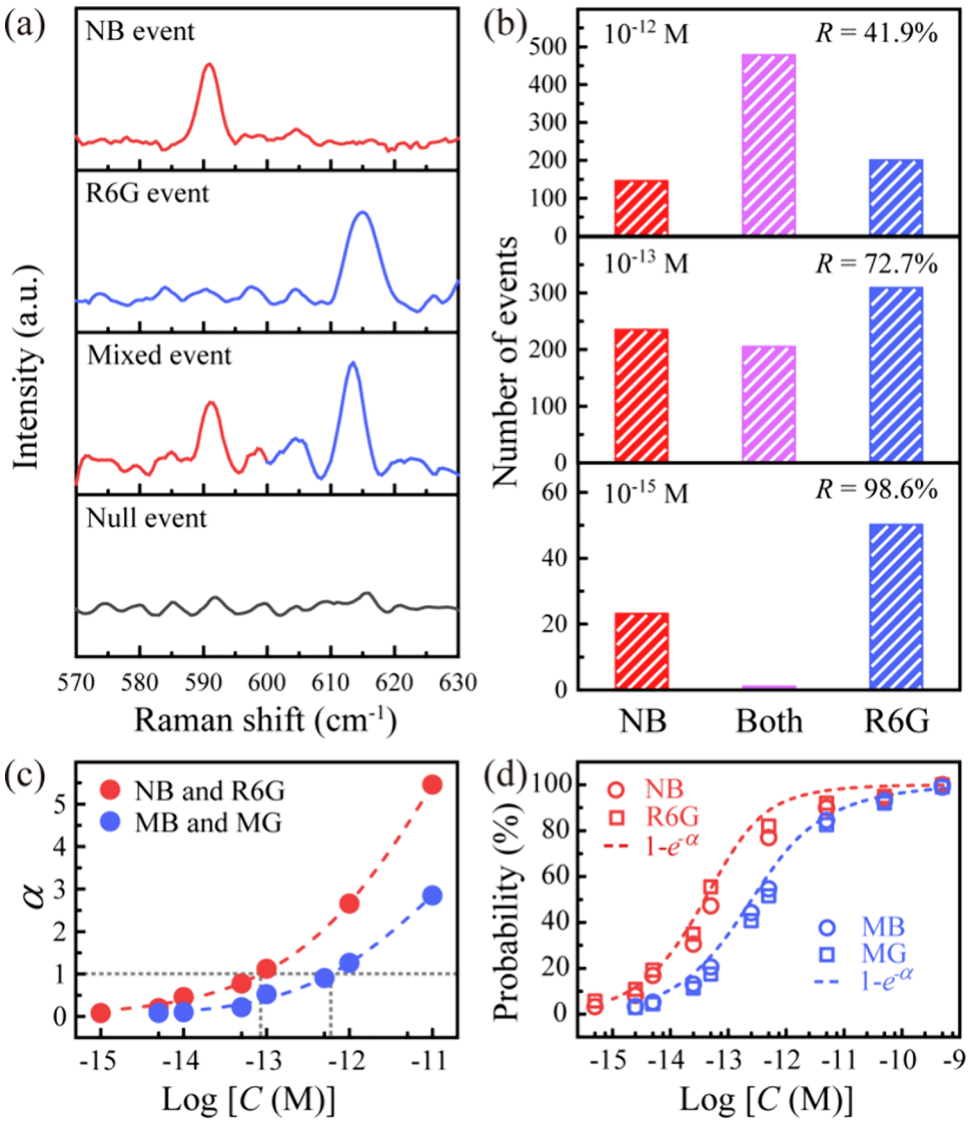

Figure 3. SERS probability and bianalyte analysis. (a) Four typical spectra for NB/R6G bianalyte measurements under the concentration of 10^{-14} M. From top to bottom: spectra of pure NB (featured at 590 cm^{-1}), pure R6G (614 cm^{-1}), mixed event with signals from both NB and R6G, and null event without effective signal. (b) Histograms of effective events for NB/R6G mixture concentrations of 10^{-12} M, 10^{-13} M, and 10^{-15} M, respectively. (c) Average number of molecules per spectrum α as a function of mixture concentration. Red dots and blue dots represent the results of NB/R6G and MB/MG in bianalyte experiments, respectively. Dotted lines indicate the concentration threshold of the SM-SERS. (d) SERS probability as a function of the concentration for different molecules. Red dots: NB (circle) and R6G (square). Blue dots: MB (circle) and MG (square). Dashed lines: $1 - e^{-\alpha}$ for NB/R6G (red) and MB/MG (blue).

$$P = \sum_{n=1}^{\infty} p(n, \alpha) = \sum_{n=0}^{\infty} p(n, \alpha) - p(0, \alpha) = 1 - e^{-\alpha} \quad (1)$$

where $\sum_{n=0}^{\infty} p(n,\alpha) = 1$ is the normalization condition. To verify this relation, we correlated the measured SERS probability P with α determined from bianalyte analysis. Nile blue (NB) and rhodamine 6G (R6G) molecules are usually used as a bianalyte pair. They feature Raman peaks at 590 and 614 cm^{-1}, respectively, with Raman intensity ratio $I_{590}/I_{614} \approx 1{:}1.7$ under 532 nm excitation (Figure S7).[48] SERS mappings were performed over 3D aggregates at different concentrations of NB/R6G mixtures (mapping area $30 \times 30\ \mu m^2$ with step 1 μm, mapping data in Figure S8). 900 pixels in SERS mapping were categorized according to their spectral signals (Figure 3a): pixels with individual Raman signals of pure NB (N_{NB}) and pure R6G (N_{R6G}), with mixed signals of both NB and R6G (N_{both}), and with neither NB nor R6G signals (N_{null}). The histograms of N_{NB}, N_{R6G} and N_{both} (Figure 3b) show that, for the mixture concentration of 10^{-12} M, most of the effective pixels have SERS signals from both molecules, while for the extremely diluted case of 10^{-15} M, almost all effective pixels were contributed by individual signals from either NB or R6G. When both analytes have similar Raman cross sections and adsorption characteristics, the experimentally obtained ratio $R = \frac{N_{NB} + N_{R6G}}{N_{NB} + N_{R6G} + N_{both}}$ is usually used to ascertain the average number of molecules in a spectrum α by $R = \frac{2}{1 + e^{\alpha/2}}$ according to Poisson distribution. To treat the case of NB and R6G with different Raman cross sections, we derived a general expression:[40]

https://doi.org/10.1021/acs.nanolett.4c03507
Nano Lett. 2024, 24, 11116−11123

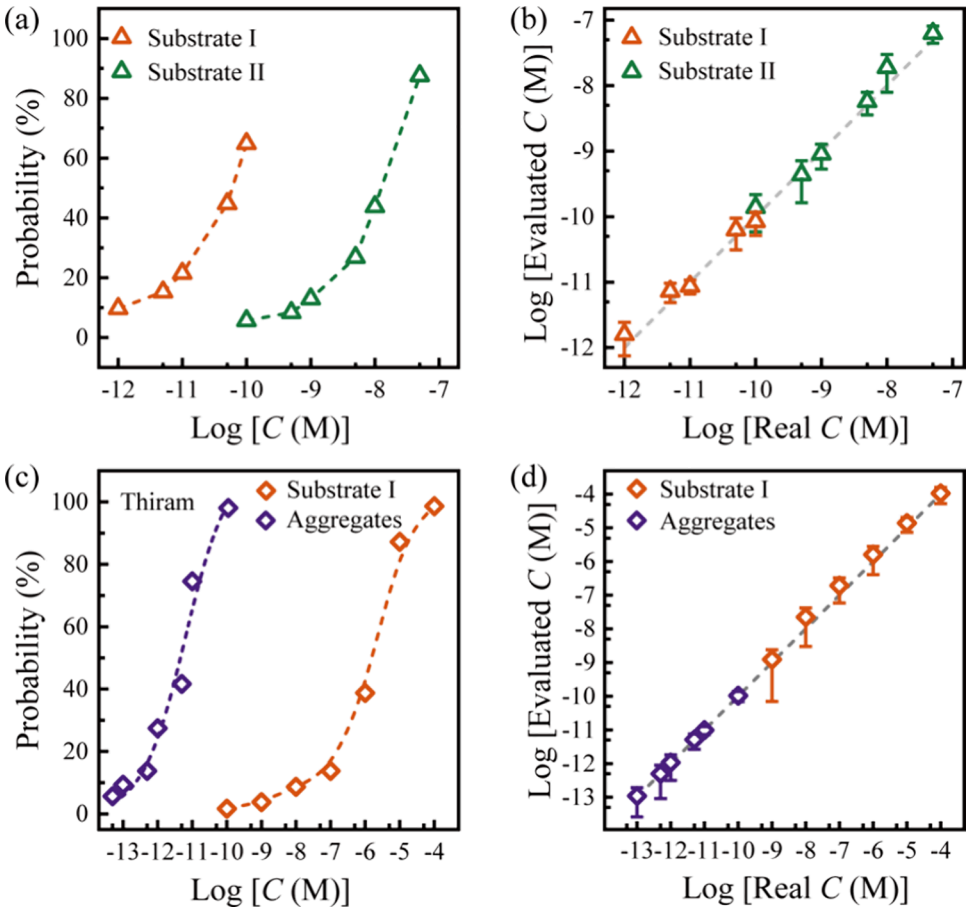

Figure 4. SERS probability and quantitative detection using commercial SERS substrates. (a) SERS probability of CV (914 cm^{-1}) as a function of concentration for two types of commercial substrates. Orange triangles: substrate I; Green triangles: substrate II. (b) SERS quantitation of the CV solution by probability calibration. SERS probability of CV at different concentrations was obtained from 900 SERS spectra with mapping area 30 × 30 μm^2 and step size 1 μm. (c) SERS probability of thiram (556 cm^{-1}) as a function of concentration using 3D nanoparticle aggregates and substrate I. Purple rhombus: 3D Aggregates; Orange rhombus: substrate I. (d) The corresponding SERS quantitation of thiram solution by probability calibration. The dashed lines in panels a and c are plotted for guiding the eyes. The gray dashed lines in panels b and d represent $y = x$. The error bars in panels b and d are standard deviations obtained from four evaluations.

$$\alpha = \ln \frac{(1 - A_1)(1 - A_2)}{A_1 A_2} \tag{2}$$

where A_1 and A_2 are the percentages of each analyte in effective SERS spectra defined as: $A_1 = N_{NB}/(N_{NB}+N_{R6G}+N_{both})$ and $A_2 = N_{R6G}/(N_{NB}+N_{R6G}+N_{both})$, respectively. The analytical derivation is described in the Supporting Information, and the contour map of α as functions of A_1 and A_2 is shown in Figure S9. The red dots in Figure 3c show the α extracted from the experimental mapping data (Figure S8) for different concentrations of the NB and R6G mixture. At concentrations of 10^{-12} M to 10^{-11} M, only a few molecules contribute to the SERS spectra. When the mixture is extremely diluted to 10^{-15} M, the average number of molecules per SERS spectrum is statistically smaller than 1. The red hollow dots in Figure 3d show the SERS probability of acquiring effective NB or R6G signals obtained from the mapping data using the expression $P = \frac{N_{effective}}{N_{effective} + N_{null}}$, where $N_{effective} = N_{both} + N_{NB}$ (N_{R6G}). As can be seen, the experimental SERS probability P is well reproduced by $1 - e^{-\alpha(C)}$ for both NB and R6G (red dashed line). More bianalyte measurements using methylene blue (MB) and malachite green (MG) were carried out to further confirm this relation. MB and MG have similar Raman intensity $I_{MB}/I_{MG} \sim 1{:}1.2$, with Raman peaks at 767 and 800 cm^{-1}, respectively (Figure S10), while their Raman cross sections are much smaller than NB/R6G. The α for MB/MG at different concentrations are presented in Figure 3c (blue dots). The experimental values of P for MB and MG again follow the relation $P = 1 - e^{-\alpha(C)}$, as shown by the blue hollow dots and blue dashed line in Figure 3d. This relation connects the macroscopic statistical SERS probability with the microscopic average molecule number in a spectrum, which indicates the microscopic essence of the SERS probability.

The threshold of SM-SERS concentration can be determined when the average number of molecules in a spectrum is $\alpha \leq 1$. For NB/R6G, SMD occurs below 0.9×10^{-13} M, as indicated by the left vertical dotted line in Figure 3c, which is consistent with previous reports in the single-molecule region using packed nanoparticles.[43,49] Furthermore, the single-molecule behavior was also confirmed by the observation of blinking at 10^{-14} M (Figure S11).[50] For the MB/MG case, the concentration threshold of SMD is 5.9×10^{-13} M, which is higher than the case of NB/R6G. This observation can be attributed to the fact that MB/MG have much smaller Raman cross sections than NB/R6G molecules. SMD occurs at hot spots with higher enhancement whose proportion is much lower.[16] Hence, a higher concentration is needed to ensure the

https://doi.org/10.1021/acs.nanolett.4c03507
Nano Lett. 2024, 24, 11116−11123

occupation of at least one molecule in these hot spots. For CV and PATP, the concentration threshold of SMD can be ascertained at 2×10^{-13} M and 8×10^{-13} M, respectively (dashed arrows in Figure 2a). In both cases, quantitative analysis (10^{-15} M for CV and 10^{-14} M for PATP) is achieved for concentrations about 2 orders of magnitude lower than the SMD threshold.

The accomplishment of SM-SERS quantitation and its physical insights presented above offer a unique methodology to implement quantitative SERS through statistical probability. We further showed that the statistical quantitation approach is universally applicable to various SERS substrates. Depending on the enhancement ability of the substrates, the SERS probability−concentration calibration curves can be established to cover different concentration ranges. As shown in Figure 4a, two commercial SERS substrates purchased from Ocean Optics (substrate I) and Integrated Optics (substrate II) were tested. These substrates were composed of silver nanoparticles with average size of 80 and 165 nm, respectively (Figure S12). Quantitative analysis of CV was successfully achieved for concentrations ranging from 10^{-12} to 10^{-10} M for substrate I and 10^{-10} to 10^{-7} M for substrate II (Figure 4b). Hence, by properly selecting SERS substrates, statistical quantitative SERS through probability can be a powerful ultrasensitive quantitative spectroscopy tool, covering a wide detection range for chemical or biomedical sensing. We take thiram, a broad-spectrum pesticide widely used to protect fruit trees from fungal diseases, as an application example. Utilizing our 3D aggregates with single-molecule sensitivity and commercial substrates with moderate enhancement, quantitation of thiram from 10^{-13} to 10^{-4} M was achieved, covering 9 orders of magnitude (Figure 4c,d). Here, we also corroborated the SMD by observing the spectral blinking behavior of thiram at 10^{-12} M (Figure S13). The quantitative detection of thiram as low as 10^{-13} M is indeed below the single-molecule threshold.

In summary, we have revealed that the statistical SERS probability P contains the microscopic information about the average number of molecules in the SERS spectrum, α, and proved a generalized relation, $P(C) = 1 - e^{-\alpha(C)}$ by bianalyte analysis. Utilizing 3D silver nanoparticle aggregates, various molecules were successfully quantified with detection limits much lower than their SMD threshold. The robustness of this statistical SERS quantitation approach was demonstrated through reproducible evaluations on different batches of solutions. Moreover, this approach is applicable to various SERS substrates, enabling chemical or biomedical detection with an extremely wide concentration range and ultrahigh sensitivity beyond single-molecule level. These results not only deepen the understanding of the statistical nature of SM-SERS but also bring a new SM-SERS/SERS quantitation tool for ultrasensitive detection and analysis.

It is noted that after the submission of our manuscript, we became aware of a newly published paper reporting quantitative SERS detection by statistical single-molecule counting.[51]

■ ASSOCIATED CONTENT

Supporting Information

The Supporting Information is available free of charge at https://pubs.acs.org/doi/10.1021/acs.nanolett.4c03507.

Detailed synthesis and experimental methods, evaluation of α by general bianalyte SERS method, and Figures S1−S13 showing additional results (PDF)

■ AUTHOR INFORMATION

Corresponding Authors

Zhipeng Li − *Beijing Key Laboratory for Nano-Photonics and Nano-Structure (NPNS), Department of Physics, Capital Normal University, Beijing 100048, China;* orcid.org/0000-0002-1946-5639; Email: zpli@cnu.edu.cn

Hongxing Xu − *School of Physics and Technology and Key Laboratory of Artificial Micro- and Nano-structures of Ministry of Education and School of Microelectronics, Wuhan University, Wuhan 430072, China; Wuhan Institute of Quantum Technology, Wuhan 430206, China; Henan Academy of Sciences, Zhengzhou 450046, China;* orcid.org/0000-0002-1718-8834; Email: hxxu@whu.edu.cn

Authors

Hao Zhang − *Beijing Key Laboratory for Nano-Photonics and Nano-Structure (NPNS), Department of Physics, Capital Normal University, Beijing 100048, China;* orcid.org/0000-0002-2755-165X

Longkun Yang − *Beijing Key Laboratory for Nano-Photonics and Nano-Structure (NPNS), Department of Physics, Capital Normal University, Beijing 100048, China;* orcid.org/0000-0002-4378-3717

Meng Zhang − *Beijing Key Laboratory for Nano-Photonics and Nano-Structure (NPNS), Department of Physics, Capital Normal University, Beijing 100048, China*

Hong Wei − *Beijing National Laboratory for Condensed Matter Physics, Institute of Physics, Chinese Academy of Sciences, Beijing 100190, China;* orcid.org/0000-0002-3616-0386

Lianming Tong − *Center for Nano-chemistry, Beijing Science and Engineering Center for Nanocarbons, Beijing National Laboratory for Molecular Sciences, College of Chemistry and Molecular Engineering, Peking University, Beijing 100871, China;* orcid.org/0000-0001-7771-4077

Complete contact information is available at: https://pubs.acs.org/10.1021/acs.nanolett.4c03507

Author Contributions

#H.Z. and L.Y. contributed equally to this work. Z.L. and H.Z. conceived the idea and initiated this route. H.Z. and M.Z. fabricated samples and carried out Raman measurements under the supervision of Z.L. and L.Y. H.X., Z.L., H.W., and L.T. analyzed the data. H.Z., L.Y., H.W., and Z.L. wrote the manuscript. All authors participated in the discussions of the results.

Notes

The authors declare no competing financial interest.

■ ACKNOWLEDGMENTS

This work was supported by the National Key Research and Development Program of China (2021YFA1400800); Beijing Natural Science Foundation (Z240005); National Key Research and Development Program of China (2021YFA1401100, 2021YFA1201500); National Natural Science Foundation of China (12374028, U22A6005, 12074421); and National Youth Talent Support Program.

REFERENCES

(1) Hwang, J.-H.; Park, S.; Son, J.; Park, J. W.; Nam, J.-M. DNA-engineerable ultraflat-faceted core-shell nanocuboids with strong, quantitative plasmon-enhanced fluorescence signals for sensitive, reliable microrna detection. *Nano Lett.* **2021**, *21*, 2132−2140.

(2) Zhang, Y.; Zhen, Y. R.; Neumann, O.; Day, J. K.; Nordlander, P.; Halas, N. J. Coherent anti-stokes Raman scattering with single-molecule sensitivity using a plasmonic fano resonance. *Nat. Commun.* **2014**, *5*, 4424.

(3) Zong, C.; Xu, M.; Xu, L. J.; Wei, T.; Ma, X.; Zheng, X. S.; Hu, R.; Ren, B. Surface-enhanced Raman spectroscopy for bioanalysis: Reliability and challenges. *Chem. Rev.* **2018**, *118*, 4946−4980.

(4) Lee, W.; Kang, B. H.; Yang, H.; Park, M.; Kwak, J. H.; Chung, T.; Jeong, Y.; Kim, B. K.; Jeong, K. H. Spread spectrum SERS allows label-free detection of attomolar neurotransmitters. *Nat. Commun.* **2021**, *12*, 159.

(5) Sharafeldin, M.; James, T.; Davis, J. J. Open circuit potential as a tool for the assessment of binding kinetics and reagentless protein quantitation. *Anal. Chem.* **2021**, *93*, 14748−14754.

(6) Hindson, C. M.; Chevillet, J. R.; Briggs, H. A.; Gallichotte, E. N.; Ruf, I. K.; Hindson, B. J.; Vessella, R. L.; Tewari, M. Absolute quantification by droplet digital PCR versus analog real-time PCR. *Nat. Methods* **2013**, *10*, 1003−1005.

(7) Xu, H.; Bjerneld, E. J.; Käll, M.; Börjesson, L. Spectroscopy of single hemoglobin molecules by surface enhanced Raman scattering. *Phys. Rev. Lett.* **1999**, *83*, 4357−4360.

(8) Esteban, R.; Baumberg, J. J.; Aizpurua, J. Molecular optomechanics approach to surface-enhanced Raman scattering. *Acc. Chem. Res.* **2022**, *55*, 1889−1899.

(9) Tian, S.; Neumann, O.; McClain, M. J.; Yang, X.; Zhou, L.; Zhang, C.; Nordlander, P.; Halas, N. J. Aluminum nanocrystals: A sustainable substrate for quantitative SERS-based DNA detection. *Nano Lett.* **2017**, *17*, 5071−5077.

(10) Lim, D. K.; Jeon, K. S.; Hwang, J. H.; Kim, H.; Kwon, S.; Suh, Y. D.; Nam, J. M. Highly uniform and reproducible surface-enhanced Raman scattering from DNA-tailorable nanoparticles with 1-nm interior gap. *Nat. Nanotechnol.* **2011**, *6*, 452−460.

(11) Yan, W. J.; Yang, L. K.; Chen, J. N.; Wu, Y. Q.; Wang, P. J.; Li, Z. P. In situ two-step photoreduced SERS materials for on-chip single-molecule spectroscopy with high reproducibility. *Adv. Mater.* **2017**, *29*, No. 1702893.

(12) Wang, X.; Huang, S.-C.; Hu, S.; Yan, S.; Ren, B. Fundamental understanding and applications of plasmon-enhanced Raman spectroscopy. *Nat. Rev. Phys.* **2020**, *2*, 253−271.

(13) Lim, D.-K.; Jeon, K.-S.; Kim, H. M.; Nam, J.-M.; Suh, Y. D. Nanogap-engineerable Raman-active nanodumbbells for single-molecule detection. *Nat. Mater.* **2010**, *9*, 60−67.

(14) Dong, L.; Yang, X.; Zhang, C.; Cerjan, B.; Zhou, L.; Tseng, M. L.; Zhang, Y.; Alabastri, A.; Nordlander, P.; Halas, N. J. Nanogapped Au antennas for ultrasensitive surface-enhanced infrared absorption spectroscopy. *Nano Lett.* **2017**, *17*, 5768−5774.

(15) Kim, J.; Kim, J. M.; Choi, K.; Park, J. E.; Nam, J. M. Open cross-gap gold nanocubes with strong, large-area, symmetric electromagnetic field enhancement for on-particle molecular-fingerprint Raman bioassays. *J. Am. Chem. Soc.* **2024**, *146*, 14012−14021.

(16) Fang, Y.; Seong, N.-H.; Dlott, D. D. Measurement of the distribution of site enhancements in surface-enhanced Raman scattering. *Science* **2008**, *321*, 388−392.

(17) Xu, H.; Aizpurua, J.; Käll, M.; Apell, P. Electromagnetic contributions to single-molecule sensitivity in surface-enhanced Raman scattering. *Phys. Rev. E* **2000**, *62*, 4318−4324.

(18) Zhu, W.; Esteban, R.; Borisov, A. G.; Baumberg, J. J.; Nordlander, P.; Lezec, H. J.; Aizpurua, J.; Crozier, K. B. Quantum mechanical effects in plasmonic structures with subnanometre gaps. *Nat. Commun.* **2016**, *7*, 11495.

(19) Schnell, M.; García-Etxarri, A.; Huber, A. J.; Crozier, K.; Aizpurua, J.; Hillenbrand, R. Controlling the near-field oscillations of loaded plasmonic nanoantennas. *Nat. Photonics* **2009**, *3*, 287−291.

(20) Shegai, T.; Li, Z.; Dadosh, T.; Zhang, Z.; Xu, H.; Haran, G. Managing light polarization via plasmon-molecule interactions within an asymmetric metal nanoparticle trimer. *Proc. Natl. Acad. Sci. U.S.A.* **2008**, *105*, 16448−16453.

(21) Park, J.-E.; Lee, Y.; Nam, J.-M. Precisely shaped, uniformly formed gold nanocubes with ultrahigh reproducibility in single-particle scattering and surface-enhanced Raman scattering. *Nano Lett.* **2018**, *18*, 6475−6482.

(22) Langer, J.; et al. Present and future of surface-enhanced Raman scattering. *ACS Nano* **2020**, *14*, 28−117.

(23) Bell, S. E. J.; Charron, G.; Cortés, E.; Kneipp, J.; de la Chapelle, M. L.; Langer, J.; Procházka, M.; Tran, V.; Schlücker, S. Towards reliable and quantitative surface-enhanced Raman scattering (SERS): From key parameters to good analytical practice. *Angew. Chem., Int. Ed.* **2020**, *59*, 5454−5462.

(24) Le Ru, E. C.; Grand, J.; Sow, I.; Somerville, W. R. C.; Etchegoin, P. G.; Treguer-Delapierre, M.; Charron, G.; Félidj, N.; Lévi, G.; Aubard, J. A scheme for detecting every single target molecule with surface-enhanced Raman spectroscopy. *Nano Lett.* **2011**, *11*, 5013−5019.

(25) Wang, X.; Park, S.-G.; Ko, J.; Xiao, X.; Giannini, V.; Maier, S. A.; Kim, D.-H.; Choo, J. Sensitive and reproducible immunoassay of multiple mycotoxins using surface-enhanced Raman scattering mapping on 3D plasmonic nanopillar arrays. *Small* **2018**, *14*, No. 1801623.

(26) Tian, H. H.; Zhang, N.; Tong, L. M.; Zhang, J. In situ quantitative graphene-based surface-enhanced Raman spectroscopy. *Small Methods* **2017**, *1*, No. 1700126.

(27) Chen, H.-Y.; Lin, M.-H.; Wang, C.-Y.; Chang, Y.-M.; Gwo, S. Large-scale hot spot engineering for quantitative SERS at the single-molecule scale. *J. Am. Chem. Soc.* **2015**, *137*, 13698−13705.

(28) Kim, J.; Sim, K.; Cha, S.; Oh, J. W.; Nam, J. M. Single-particle analysis on plasmonic nanogap systems for quantitative SERS. *J. Raman Spectrosc.* **2021**, *52*, 375−385.

(29) Go, S.; Yoo, S.; Son, J.; Lee, S.; Lee, J.; Lee, S.; Kim, J.; Park, M.; Park, W.; Kim, J. M.; Nam, J. M.; Park, S. Ring-in-a-triangle nanoframes: Integrating with intra- and interhotspots for highly amplified near-field focusing. *Nano Lett.* **2022**, *22*, 1734−1740.

(30) Kim, J. M.; Kim, J.; Ha, M.; Nam, J. M. Cyclodextrin-based synthesis and host-guest chemistry of plasmonic nanogap particles with strong, quantitative, and highly multiplexable surface-enhanced Raman scattering signals. *J. Phys. Chem. Lett.* **2020**, *11*, 8358−8364.

(31) Hao, Q.; Peng, Z.; Wang, J.; Fan, X.; Li, G.; Zhao, X.; Ma, L.; Qiu, T.; Schmidt, O. G. Verification and analysis of single-molecule SERS events via polarization-selective Raman measurement. *Anal. Chem.* **2022**, *94*, 1046−1051.

(32) Lombardi, J. R.; Birke, R. L.; Haran, G. Single molecule SERS spectral blinking and vibronic coupling. *J. Phys. Chem. C* **2011**, *115*, 4540−4545.

(33) Benz, F.; Schmidt, M. K.; Dreismann, A.; Chikkaraddy, R.; Zhang, Y.; Demetriadou, A.; Carnegie, C.; Ohadi, H.; de Nijs, B.; Esteban, R.; Aizpurua, J.; Baumberg, J. J. Single-molecule optomechanics in "picocavities". *Science* **2016**, *354*, 726−729.

(34) Etchegoin, P. G.; Meyer, M.; Le Ru, E. C. Statistics of single molecule SERS signals: Is there a poisson distribution of intensities? *Phys. Chem. Chem. Phys.* **2007**, *9*, 3006−3010.

(35) de Albuquerque, C. D. L.; Sobral-Filho, R. G.; Poppi, R. J.; Brolo, A. G. Digital protocol for chemical analysis at ultralow concentrations by surface-enhanced Raman scattering. *Anal. Chem.* **2018**, *90*, 1248−1254.

(36) Dieringer, J. A.; Lettan, R. B.; Scheidt, K. A.; Van Duyne, R. P. A frequency domain existence proof of single-molecule surface-enhanced Raman spectroscopy. *J. Am. Chem. Soc.* **2007**, *129*, 16249−16256.

(37) Son, J.; Kim, G.-H.; Lee, Y.; Lee, C.; Cha, S.; Nam, J.-M. Toward quantitative surface-enhanced Raman scattering with plasmonic nanoparticles: Multiscale view on heterogeneities in particle morphology, surface modification, interface, and analytical protocols. *J. Am. Chem. Soc.* **2022**, *144*, 22337−22351.

https://doi.org/10.1021/acs.nanolett.4c03507
Nano Lett. 2024, 24, 11116−11123

(38) Le Ru, E. C.; Etchegoin, P. G.; Meyer, M. Enhancement factor distribution around a single surface-enhanced Raman scattering hot spot and its relation to single molecule detection. *J. Chem. Phys.* **2006**, *125*, No. 204701.
(39) Le Ru, E. C.; Meyer, M.; Etchegoin, P. G. Proof of single-molecule sensitivity in surface enhanced Raman scattering (SERS) by means of a two-analyte technique. *J. Phys. Chem. B* **2006**, *110*, 1944−1948.
(40) Zrimsek, A. B.; Wong, N. L.; Van Duyne, R. P. Single molecule surface-enhanced Raman spectroscopy: A critical analysis of the bianalyte versus isotopologue proof. *J. Phys. Chem. C* **2016**, *120*, 5133−5142.
(41) Blackie, E. J.; Le Ru, E. C.; Etchegoin, P. G. Single-molecule surface-enhanced Raman spectroscopy of nonresonant molecules. *J. Am. Chem. Soc.* **2009**, *131*, 14466−14472.
(42) Yang, K.; Zhu, K.; Wang, Y.; Qian, Z.; Zhang, Y.; Yang, Z.; Wang, Z.; Wu, L.; Zong, S.; Cui, Y. $Ti_3C_2T_x$ mxene-loaded 3D substrate toward on-chip multi-gas sensing with surface-enhanced Raman spectroscopy (SERS) barcode readout. *ACS Nano* **2021**, *15*, 12996−13006.
(43) Yang, S.; Dai, X.; Stogin, B. B.; Wong, T.-S. Ultrasensitive surface-enhanced Raman scattering detection in common fluids. *Proc. Natl. Acad. Sci. U.S.A.* **2016**, *113*, 268−273.
(44) Zhang, D.; Peng, L.; Shang, X.; Zheng, W.; You, H.; Xu, T.; Ma, B.; Ren, B.; Fang, J. Buoyant particulate strategy for few-to-single particle-based plasmonic enhanced nanosensors. *Nat. Commun.* **2020**, *11*, 2603.
(45) Gao, S. T.; Xiang, S. Q.; Jiang, Y. M.; Zhao, L. B. A density functional theoretical study on the charge-transfer enhancement in surface-enhanced Raman scattering. *ChemPhysChem* **2018**, *19*, 3401−3409.
(46) Jarvius, J.; Melin, J.; Göransson, J.; Stenberg, J.; Fredriksson, S.; Gonzalez-Rey, C.; Bertilsson, S.; Nilsson, M. Digital quantification using amplified single-molecule detection. *Nat. Methods* **2006**, *3*, 725−727.
(47) Le Ru, E. C.; Etchegoin, P. G.; Meyer, M. Enhancement factor distribution around a single surface-enhanced Raman scattering hot spot and its relation to single molecule detection. *J. Chem. Phys.* **2006**, *125*, 204701.
(48) Ahmed, A.; Gordon, R. Single molecule directivity enhanced Raman scattering using nanoantennas. *Nano Lett.* **2012**, *12*, 2625−2630.
(49) Yan, W. W.; Chen, S. Y.; Li, P.; Dong, R. L.; Shin, H. H.; Yang, L. B. Real-time monitoring of a single molecule in sub-nanometer space by dynamic surface-enhanced Raman spectroscopy. *J. Phys. Chem. Lett.* **2023**, *14*, 8726−8733.
(50) Etchegoin, P. G.; Meyer, M.; Blackie, E.; Le Ru, E. C. Statistics of single-molecule surface enhanced Raman scattering signals: Fluctuation analysis with multiple analyte techniques. *Anal. Chem.* **2007**, *79*, 8411−8415.
(51) Bi, X.; Czajkowsky, D. M.; Shao, Z.; Ye, J. Digital colloid-enhanced Raman spectroscopy by single-molecule counting. *Nature* **2024**, *628*, 771−775.

https://doi.org/10.1021/acs.nanolett.4c03507
Nano Lett. 2024, 24, 11116−11123